Article

Journal of
Nanoscience and Nanotechnology
Vol. 16, 11831–11838, 2016
www.aspbs.com/jnn

Etch Characteristics of SiO_2 Using Pulsed Triple-Frequency for $Ar/C_4F_6/O_2$ Capacitive Coupled Plasmas

M. H. Jeon[1], J. W. Park[2], T. H. Kim[2], D. H. Yun[2], K. N. Kim[3], and G. Y. Yeom[1,2,*]

[1] *SKKU Advanced Institute of Nano Technology (SAINT), Sungkyunkwan University, Suwon, Gyeonggi-do 440-746, South Korea*
[2] *Department of Advanced Materials Science and Engineering, Sungkyunkwan University, Suwon, Gyeonggi-do 440-746, South Korea*
[3] *School of Advanced Materials Science and Engineering, Daejeon University, Daejeon, 330-716, South Korea*

We investigated the effects of 13.56 MHz radio frequency (rf) power as a medium frequency power on the plasma characteristics and etch properties of an amorphous carbon layer (ACL) and SiO_2, using $Ar/C_4F_6/O_2$ gas mixtures in a capacitively coupled plasma (CCP) system operated with pulsed superimposed triple-frequency power of 60 MHz (source)/13.56 MHz (bias)/2 MHz (bias). Compared to the dual frequency rf power of 13.56 MHz (400 W)/2 MHz (900 W) or 60 MHz (400 W)/2 MHz (900 W), the use of triple-frequency rf power of 60 MHz/13.56 MHz/2 MHz (900 W) showed a better anisotropic SiO_2 etch profile, with the higher etch selectivity of SiO_2 over the ACL. We observed the best SiO_2 etch characteristics when the rf powers of 60 MHz and 13.56 MHz were set as 60 MHz (200 W)/13.56 MHz (200 W). In addition, when we varied the pulse duty percentage of 13.56 MHz rf power from 25∼100% (continuous wave (CW)), while keeping the rf powers of 60 MHz/13.56 MHz/2 MHz at 200 W/200 W/900 W, respectively, and while maintaining the pulse duty percentage of 60 MHz and 2 MHz at 50%, the use of the synchronized pulse on/off condition (i.e., the use of 50% duty percentage of 13.56 MHz) also showed the best etch characteristics. The best SiO_2 etch characteristics and the highest etch selectivity of SiO_2 over the ACL (observed for both rf power ratios of 60 MHz (200 W)/13.56 MHz (200 W), and for the triple-frequency pulsing with the synchronized pulse on/off) were related to the higher CF_x/F ratios, which increased the fluorocarbon polymer passivation on the ACL surface and SiO_2 sidewall during etching.

Keywords: Synchronized RF Power, Puled Plasma Etching, RF Frequency Effect, Selective Etching.

1. INTRODUCTION

For nanoscale dynamic random access memories (DRAMs), the feature sizes of the devices are scaled down to nanoscale without increasing or changing the heights of materials (e.g., the thickness of the contact SiO_2, or the height of the storage node capacitor) to compensate for the capacitance value for operating the device with high reliability, etc.[1–3] As such, plasma etching is becoming one of the most important processes for nanoscale semiconductor manufacturing. Especially for next generation nanoscale semiconductor device fabrication, precise etch process control needs to be achieved, in addition to a solution to certain problems (e.g., etch stop, low etch uniformity, pattern distortion, physical damages induced by charge unbalance, etc.) that are observed during the etching of nanoscale patterns using conventional plasma etching techniques.[4–6]

As one of the next generation plasma etch techniques for the improved control of etch processes, the pulsed plasma technique has been introduced, in which the etch properties are adjusted by turning the rf powers on and off during the etching. The main advantages of pulsed plasma processes reported in the literature are the improvement in etch selectivity and the reduction of charging

*Author to whom correspondence should be addressed.

damages and defects, by controlling the effective gas dissociation characteristics in the plasma and by reducing the electron shading phenomena, respectively.[7–10] By varying the pulse parameters (e.g., the pulse duty ratio and pulse frequency) during etching, the plasma properties alter to become more flexible.[11, 12] Also, through dual source/bias pulsing and synchronization, more independent control of the plasma characteristics (e.g., plasma chemical composition and ion bombardment energy) has been achieved, allowing for more precise control of the etch process.[13–15]

Today, synchronized pulse dual frequency capacitive coupled plasma (DF-CCP) systems are widely investigated for nano pattern etch processing.[14–17] In general, the source power is operated with a very high frequency (VHF) (above 40 MHz), while the bias power is operated with a low frequency (up to a few MHz) in the DF-CCP. However, during synchronized dual frequency operation, a further decrease of the SiO_2 etch rate has been generally observed, together with a simultaneous improvement of the etch profiles, due to the increased etch selectivity over the hard mask layer.[18, 19] If the duty percentage is increased to increase the SiO_2 etch rates during synchronized pulsing, etch selectivity is decreased, degrading the etch profile. To improve the etch characteristics further without decreasing the SiO_2 etch rate, an additional rf power (with a frequency range between very high frequency (VHF) source and low frequency bias) has also been used as a third rf power to form a triple-frequency pulsed plasma system. However, the effects of the mid-frequency on the plasma properties and etch characteristics during the operation of a triple-frequency pulsed plasma system are not well understood and need further investigation.

In this study, we investigated the characteristics of superimposed triple rf pulsed CCPs obtained by applying a pulsed 60 MHz power on the top electrode as a source power and a pulsed 13.56 MHz/2 MHz power on the bottom substrate electrode as a bias power with an $Ar/C_4F_6/O_2$ gas mixture. With the triple rf pulsed CCP, we investigated the effects of 13.56 MHz (mid-frequency power to the substrate) on the plasma properties and SiO_2 etch characteristics (e.g., etch selectivity and etch profile).

2. EXPERIMENTAL DETAILS

The experimental setup of the superimposed triple-frequency pulsed CCP system used in this study is shown in Figure 1. The rf discharge was maintained between the two parallel plate electrodes separated by 30 mm. The top electrode was covered with a perforated silicon plate to flow gases uniformly and was connected to a pulsed 60 MHz rf power (VHF) source to control the plasma characteristics. The etch gases were equally distributed through a baffle system from the top electrode. The bottom substrate electrode was water-cooled and connected to two pulsed rf powers of 13.56 MHz and 2 MHz. These 13.56 MHz and 2 MHz rf powers were generated using two signal generators (8657B, HP) and two rf power amplifiers (A1000, ENI), and the pulsing of these two rf frequency powers was synchronized with the pulsing of the 60 MHz rf power using a digital delay generator (DG 645, SRS) to form a synchronized triple rf pulsing system.

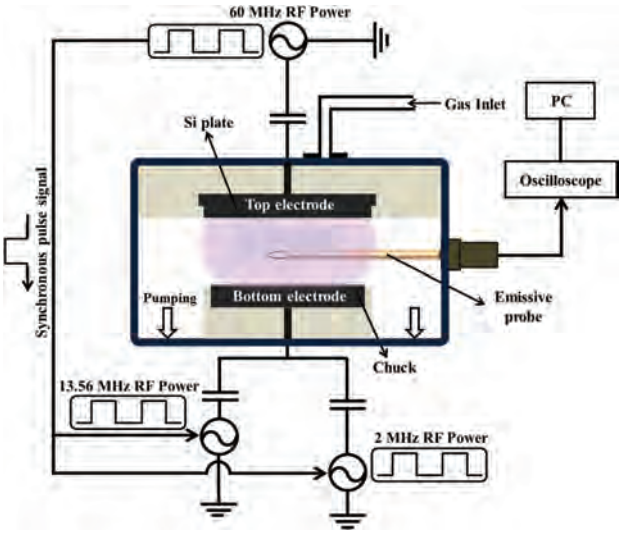

Figure 1. Schematic diagram of synchronized rf pulsing in the triple-frequency CCP. A pulsed 60 MHz source power was applied to the top electrode to control the plasma properties. Pulsed 13.56/2 MHz bias powers were applied to the bottom electrode to control both the plasma properties and ion energy at the substrate.

We used a 2-μm thick SiO_2 layer deposited on silicon wafers, masked with a 600-nm thick amorphous carbon layer (ACL), as samples. The SiO_2 layer was etched as a function of the different power ratios of 60 MHz/13.56 MHz; meanwhile, maintaining the power of 60 MHz + 13.56 MHz at 400 W and the 2 MHz rf power at 900 W, as a function of the pulse duty percentages of 13.56 MHz medium frequency, and while keeping the 60/13.56/2 MHz of triple frequency rf power at 200 W/200 W/900 W, respectively. The pulse frequency was also maintained at 1 kHz, and the gas chemistry of $Ar/C_4F_6/O_2 = 150/40/10$ sccm was used at a process pressure of 30 mTorr as the etch gas mixture.

The etch characteristics of the SiO_2 layer on ACL were estimated by field emission scanning electron microscopy (FE-SEM, Hitachi S-4700). The instant change of the electron temperature for the triple-frequency pulse conditions of the 60/13.56/2 MHz pulsing system was calculated using an emissive probe. The radicals which dominantly affect the etching were observed using time-resolved optical emission spectroscopy (OES, Andoristar 734). The time-resolved OES characteristics were investigated using a spectrometer composed of a grating monochromator and an intensified charge-coupled device (ICCD). For the time-resolved data collection, the OES data were collected with an interval of 100 μs in the 1 kHz pulse period, and the data were averaged 10 times after the collection. Also, the

chemical compositions on the etched SiO_2 surface were observed using X-ray photoelectron spectroscopy (XPS, ESCA2000, VG Microtech Inc.) to investigate the chemical binding characteristics.

3. RESULTS AND DISCUSSION

To investigate the effect of 13.56 MHz rf power during the operation of the triple-frequency pulse CCPs, the ratio of the high frequency 60 MHz rf power to the medium 13.56 MHz rf power, was varied while maintaining the low 2 MHz rf power. The effects of the ratios on the plasma properties were then investigated. First, the power ratios of 60 MHz/13.56 MHz were varied from 400 W/0 W to 0 W/400 W, while maintaining the power of 60 MHz + 13.56 MHz at 400 W, the 2 MHz rf power at 900 W, the pulse frequency at 1 kHz, and the pulse duty percentage at 50%. 150 sccm Ar was used at a pressure of 30 mTorr. Using an emissive probe, the variation of instant electron temperature was calculated after measurement of instant plasma potentials (V_p, measured at a heated temperature) and instant floating potentials (V_f, measured the room temperature) using the following equation.[19]

$$V_p - V_f = \frac{kT_e}{2e} \ln\left(\frac{2M}{\pi m}\right)$$

where k was the Boltzmann constant, T_e was the electron temperature, m was the electron mass, and M was the atomic mass of Ar gas. The results are shown in Figure 2 for 400 W/0 W, 300 W/100 W, 200 W/200 W, 100 W/300 W, and 0 W/400 W of 60 MHz/13.56 MHz, respectively. As shown in Figure 2, during the pulse-on time (0∼500 μs), high electron temperatures in the range of 5.3∼8.0 eV were observed and after the pulse-off (500∼1000 μs), the electron temperature exponentially decreased to 0 eV due to no power. Especially, immediately after the pulse-on time, an overshoot of electron temperature to about 10∼12 eV (9.5, 10.1, 10.3, 11.4, and 11.8 eV for 400 W/0 W, 300 W/100 W, 200 W/200 W, 100 W/300 W, and 0 W/400 W of 60 MHz/13.56 MHz, respectively) was observed. Previous research showed that the overshoot of electron temperature of the source plasma (during the synchronized dual frequency pulsing) decreased the SiO_2 etch selectivity (over ACL) and degraded the SiO_2 etch profile (masked with ACL) by increasing the gas dissociation of C_4F_6.[20] For this synchronized triple frequency pulsing experiment, an overshoot of electron temperature was also observed similar to the synchronized dual frequency pulsing due to the synchronized initial pulsing of source power and bias power. For the pulse-on period, depending on an rf power ratio of 60 MHz/13.56 MHz, the electron temperature increased from 5.3 eV for 400 W/0 W to 8.0 eV for 0 W/400 W.

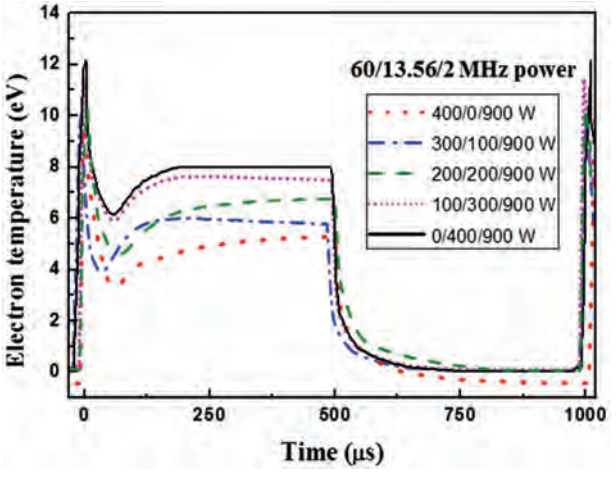

Figure 2. Instant electron temperature estimated as a function of the 60/13.56 MHz rf power ratios in the synchronously pulsed plasmas. Ar gas at an operating pressure of 30 mTorr was used. The pulse duty ratio and the pulse frequency were kept at 50% and 1 kHz, respectively. 60/13.56/2 MHz rf powers were varied as 400/0/900 W, 300/100/900 W, 200/200/900 W, 100/300/900 W, and 0/400/900 W, respectively.

Based on the instant electron temperature characteristics for the different power ratios of 60 MHz/13.56 MHz, the temporal gas dissociation characteristics were investigated using the time-resolved OES for the reactive gas mixture of $Ar/C_4F_6/O_2$ = 150/40/10 sccm used to etch SiO_2. Other process conditions were maintained the same as those shown in Figure 2. Radical species related to the SiO_2 etching such as CF_2 (235∼255 nm), CF_3 (255∼275 nm), F (703 nm), and Ar (751 nm) were observed. The optical emission intensity ratios of CF_2/Ar and F/Ar as the estimation of dissociated radical concentration and the radical ratio of CF_2/F, which is related to fluorocarbon polymerization, were measured and the results are shown in Figures 3(a∼c) for 400 W/0 W, 300 W/100 W, 200 W/200 W, 100 W/300 W, and 0 W/400 W of 60 MHz/13.56 MHz, respectively. The signals were measured every 100 μs in the range of 0∼1000 μs. For accuracy, the data were averaged after ten times of measurement. As shown in Figures 3(a and b), during the pulse-on (0∼500 μs), high intensity of F/Ar was observed with smaller CF_2/Ar, due to the gas dissociation of C_4F_6. After the pulse-off (500∼1000 μs), the intensities decreased slowly with time, due to the recombination of radicals. Especially, during the initial pulse-on, higher F/Ar ratios were observed for some of the cases, possibly due to the initial overshoot of electron temperature. During the pulse-off, the F/Ar initially decreased faster than CF_2/Ar; therefore, the ratios of CF_2/F increased significantly with time for 100 μs (500∼600 μs), and the further increase of time slowly decreased the ratios of CF_2/F due to the recombination, shown in Figure 3(c). It is believed that the faster decrease of F/Ar compared to CF_2/Ar is related to the fact that F is only lost by the recombination with other molecules during the pulse-off time, while CF_2 can be generated during the pulse-off time by the recombination of F and CF while it can

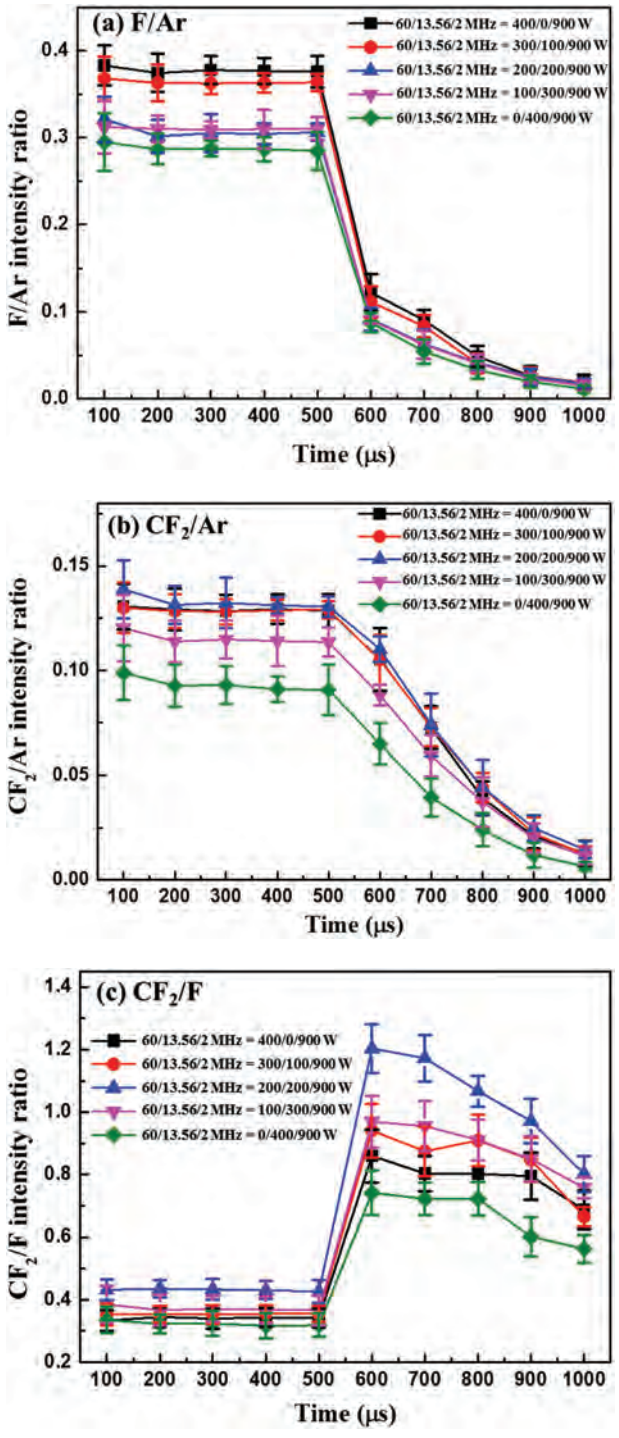

Figure 3. Time-resolved optical emission intensity ratios of (a) F/Ar, (b) CF_2/Ar and (c) CF_2/F as a function of 60/13.56 MHz rf power ratios using $Ar/C_4F_6/O_2$ gas mixtures in synchronously pulsed plasmas. The other conditions are the same as those in Figure 2.

be also lost by the recombination with other molecules. For different rf power ratios, while keeping the total 60 MHz + 13.56 MHz power at 400 W, the ratios of F/Ar and CF_2/Ar decreased with increasing 13.56 MHz rf power ratio. This phenomenon was possibly due to decreased plasma density with decreasing rf frequency, even though the electron temperature increased with the increase of 13.56 MHz, as shown in Figure 2. However, the ratio of CF_2/F increased with increasing 13.56 MHz up to 200 W/200 W of 60 MHz/13.56 MHz, while further increase of 13.56 MHz rf power decreased the CF_2/F. Therefore, the highest CF_2/F was observed for the rf power ratios of 60 MHz/13.56 MHz = 200 W/200 W. This change of CF_2/F with varying rf frequency ratios is not well understood, but it is possibly related to the different dissociation rates of F and CF_2 for different rf frequencies.

SiO_2 samples masked with ACL were etched for different rf power ratios of 60 MHz/13.56 MHz, with the process conditions shown in Figure 3. The etch profiles are shown in Figures 4(a–e) for 400 W/0 W, 300 W/100 W, 200 W/200 W, 100 W/300 W, and 0 W/400 W of 60 MHz/13.56 MHz power ratio, respectively, after the etching of about 1.6 μm of SiO_2. As shown in Figure 4, the thickness of ACL remaining after the etching of 1.6-μm thick SiO_2 increased with the increase of 13.56 MHz rf power, and showed the maximum at 200 W/200 W of 60 MHz/13.56 MHz. The further increase of 13.56 MHz rf power reduced the ACL thickness. Also, the most anisotropic SiO_2 etch profile was observed at the condition of 200 W/200 W of 60 MHz/13.56 MHz, by showing the ratio of bottom CD/top CD as 0.43 for (a), 0.40 for (b), 0.45 for (c), 0.40 for (d), and 0.39 for (e). The thickest ACL and the most anisotropic SiO_2 etch profile observed at the condition of 200 W/200 W of 60 MHz/13.56 MHz are believed to be partially related to the highest CF_2/F ratio observed at 200 W/200 W of 60 MHz/13.56 MHz as shown in Figure 4. The CF_2/F ratio was related to the formation of a fluorocarbon polymer passivation layer formed during the etching. The formation of the thickest fluorocarbon polymer layer on the top of the ACL and the sidewall of the SiO_2 reduced the etch damages such as maintaining of top CD width, minimizing of necking, bowing and bottom distortion using the condition of 200 W/200 W of 60 MHz/13.56 MHz. Therefore, the thickest ACL and the most anisotropic SiO_2 etch profile were observed.

While maintaining the 60 MHz/13.56 MHz/2 MHz rf power = 200 W/200 W/900 W, which showed the most anisotropic SiO_2 etch profile, the pulse duty percentage of 13.56 MHz was varied and the effects of the pulse duty percentage of 13.56 MHz on the characteristics of the plasma and the SiO_2 etch characteristics were further investigated. The pulsing conditions used in the experiment are shown in Figure 5 and the pulse duty percentage was varied from 100(CW) to 25%, while keeping the pulse duty percentages of 60 MHz and 2 MHz at 50%. The pulse frequency was maintained at 1 kHz. First, the temporal electron temperature was measured for different pulse duty percentages of 13.56 MHz rf power with 150 sccm Ar and at an operating pressure of 30 mTorr. The results are shown in Figure 6 for 100% (CW), 75%, 50%, and

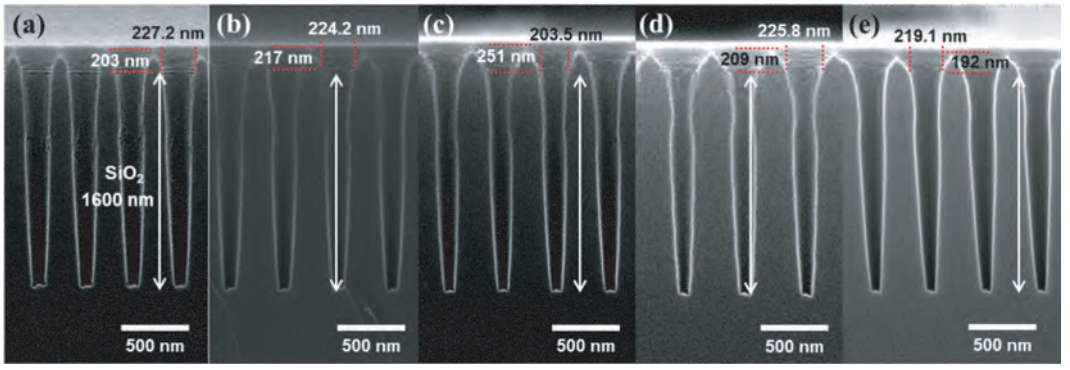

Figure 4. Etch profiles of ACL masked SiO_2 observed by FE-SEM after the etching as a function of 60/13.56 MHz rf power ratios using $Ar/C_4F_6/O_2$ gas mixtures in the pulsed triple-frequency CCP, with a pulse duty percentage of 50% and pulse frequency of 1 kHz. The etch time of SiO_2 was varied to obtain about 1.6 μm of etch depth. The process conditions are the same as those in Figures 3(a–e) for 400 W/0 W, 300 W/100 W, 200 W/200 W, 100 W/300 W, and 0 W/400 W of the 60 MHz/13.56 MHz power ratio, respectively, while keeping 2 MHz power at 900 W.

25% of 13.56 MHz pulse duty percentage. As shown in Figure 6, for 100% (CW) of 13.56 MHz, after an initial overshoot of electron temperature, the electron temperature of about 6.7 eV was observed for 0∼500 μs when 200 W/200 W/900 W of 60 MHz/13.56 MHz/2 MHz rf power was applied. For 500∼1000 μs, the electron temperature decreased to about 4.3 eV, due to being operated with 200 W of 13.56 MHz rf power only. When the duty percentage of 13.56 MHz rf power decreased to 75% and 50% for 750∼1000 μs and 500∼1000 μs, respectively, the electron temperature decreased to 0 eV, as there was no power at that period. Also, when the 13.56 MHz rf pulse percentage decreased further to 25% for 250∼500 μs, the electron temperature of about 3.7 eV was observed as the rf power was 200 W/200 W of 60 MHz/2 MHz.

For the different pulse duty percentages of 13.56 MHz shown in Figure 6, the time-resolved OES was measured using the reactive gas mixture composed of $Ar/C_4F_6/O_2$ = 150/40/10 sccm. The optical emission intensity ratios of F/Ar and CF_2/F, were measured and the results are shown in Figures 7(a and b), respectively, for 100% (CW), 75%, 50%, and 25% of 13.56 MHz pulse duty percentage. As shown in Figure 7, when 13.56 MHz rf power was always on, no significant change in the F/Ar ratio, was observed and the CF_2/F ratio was also very low since the continuous gas dissociation through the electron temperature was higher than 4 eV as shown in Figure 6. The CF_2/F ratio during the pulse-off period increased with decreasing the pulse duty percentage of 13.56 MHz up to 50%. The further decrease of 13.56 MHz rf power to 25%

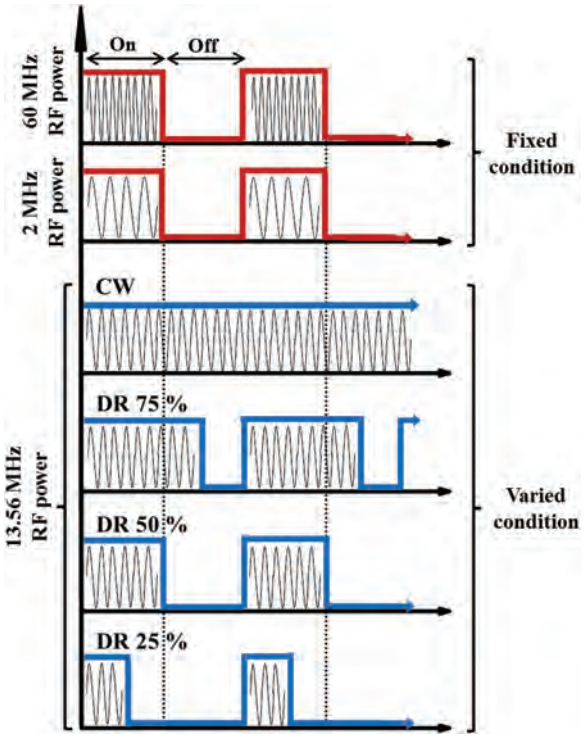

Figure 5. Schematic diagram of the pulse synchronization between the 60 MHz source pulsing and the 13.56/2 MHz bias pulsing for various 13.56 MHz pulse duty percentages in the synchronized triple-frequency CCP.

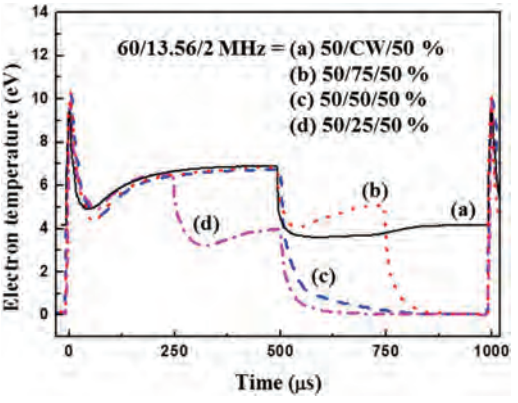

Figure 6. Instant electron temperature estimated as a function of 13.56 MHz pulse duty percentages in the synchronously pulsed plasmas. Ar gas at an operating pressure of 30 mTorr was used. The 13.56 MHz pulse duty percentage was varied from 100% (CW) to 25%, while maintaining the 60 MHz/13.56 MHz/2 MHz rf power = 200 W/200 W/900 W, respectively.

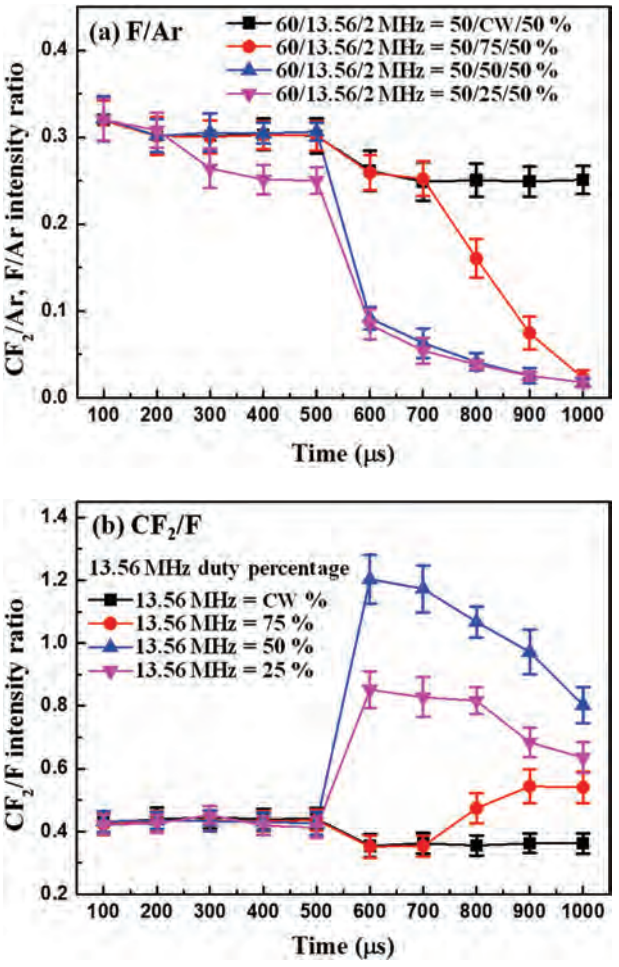

Figure 7. Time-resolved optical emission intensity ratios of (a) F/Ar and (b) CF_2/F as a function of 13.56 MHz pulse duty percentages using $Ar/C_4F_6/O_2$ gas mixtures in the synchronously pulsed plasmas. The other conditions are the same as those in Figure 6.

reduced the ratios of CF_2/F. When only one or two rf powers were on before the pulse-off such as 500∼750 μs with 200 W of 13.56 MHz only for 60/13.56/2 MHz = 50%/75%/50% and 250∼500 μs with 200 W/900 W of 60 MHz/2 MHz for 60/13.56/2 MHz = 50%/25%/50%, not only low F/Ar intensity, but also low CF_2/F ratio was observed. Therefore, the highest CF_2/F ratio during the pulse-off time was observed when the triple rf pulses were pulsed off at the same time synchronously as shown for 60/13.56/2 MHz = 50%/50%/50%.

The etch profiles of the SiO_2 samples masked with ACL were also observed after the etching of about 1.6 μm of SiO_2 for different rf power ratios of 60 MHz/13.56 MHz, with the process conditions as shown in Figure 7. The results are shown in Figures 8(a–d) for 100% (CW), 75%, 50%, and 25% of 13.56 MHz pulse duty percentage, respectively. As shown in Figure 8, the ACL thickness remaining after the etching was the thickest, the SiO_2 top hole width was the smallest, and the etch profile appeared to be the most anisotropic for 50% of the 13.56 MHz duty percentage shown in Figure 7(c) (the ratio of bottom CD/top CD was 0.38 for (a), 0.40 for (b), 0.45 for (c), 0.41 for (d), and 0.39 for (e)), which is the triple-frequency pulsing condition with the synchronized pulse on/off. At that condition, as shown in Figure 7, the CF_2/F ratio that is related to the fluorocarbon polymerization was highest during the pulse-off time.

Using XPS, the compositions of the fluorocarbon polymerization layer formed on the ACL and SiO_2 during the etching were estimated with results shown in Figures 9(a and b), respectively. Binding peaks related to C–C, CF_x ($x = 1, 2$), and C–CF were observed. As shown in Figure 9(a), with the decrease of 13.56 MHz pulse duty percentage from 100% (CW) to 50%, the C–C bonding peak intensity decreased, while the CF_x ($x = 1, 2$) bonding peak intensities increased, indicating the increased thickness of the fluorocarbon polymer layer on the surfaces of ACL. However, further decrease of the 13.56 MHz pulse duty percentage from 50% to 25% increased the C–C bonding peak intensity and decreased the CF_x ($x = 1, 2$) bonding peaks, indicating the decrease of the fluorocarbon polymer layer on the ACL. For SiO_2, as shown in Figure 9(b), similar changes of the C–C and CF_x ($x = 1, 2$) bonding peak intensities to those of ACL were observed.

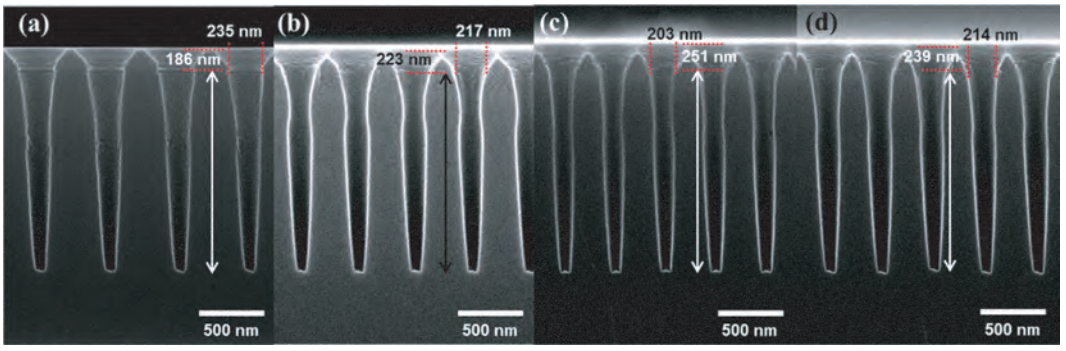

Figure 8. Etch profiles of ACL masked SiO_2 after etching as a function of 13.56 MHz pulse duty percentages in the pulsed triple-frequency CCP. The etch time of SiO_2 was varied to obtain an etch depth of about 1.6 μm. The process conditions are the same as those in Figures 7(a–d) for 100% (CW), 75%, 50%, and 25% of 13.56 MHz pulse duty percentage, respectively, while keeping the pulse duty percentages of 60 MHz and 2 MHz at 50%.

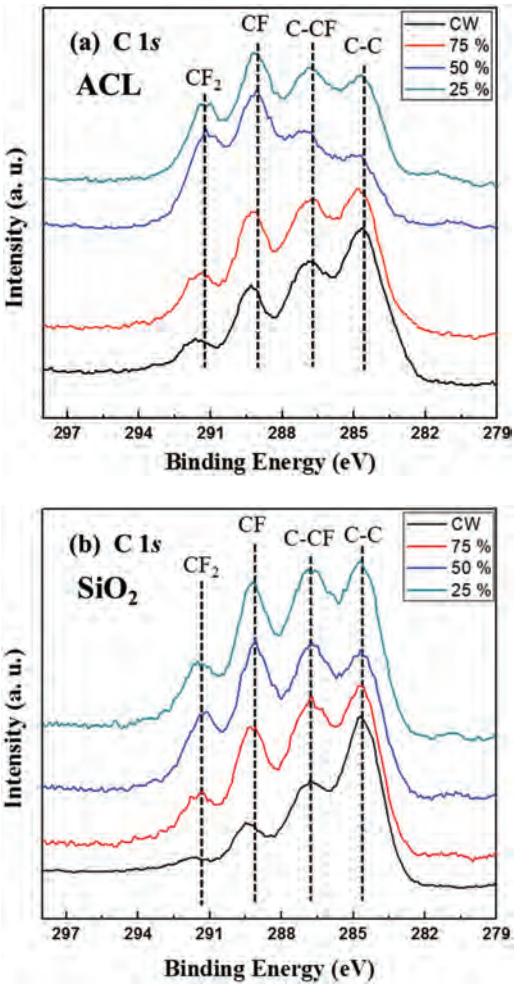

Figure 9. XPS narrow scan data of C 1*s* on the etched ACL and SiO_2 surface as a function of 13.56 MHz pulse duty percentages. SiO_2 samples were etched to 1.6 μm of etch depth in the 60/13.56/2 MHz triple-frequency CCP. The process conditions are the same as those in Figure 7.

The change of the C–C and CF_x ($x = 1, 2$) bonding peak intensities with the 13.56 MHz pulse duty percentage is related to the CF_2/F ratio observed in Figure 8 during the etching using $Ar/C_4F_6/O_2$.

The thickness values of the fluorocarbon polymer on the ACL and SiO_2 were estimated with the C 1*s* XPS narrow scan data in Figures 9(a and b), respectively, using the following equation,[21, 22]

$$d_{(\text{CF polymer})} = \lambda_{(C1s)} \ln\left(1 - \frac{I^d_{(C1s)}}{I_{(C1s)}}\right)^{-1}$$

where $d_{(\text{CF polymer})}$ was the fluorocarbon polymer layer thickness, $\lambda_{(C1s)}$ was the mean free path of C 1*s* photoelectrons (2.5 nm),[21] $I^d_{(C1s)}$ was the integrated XPS photoemission intensity of C 1*s*, and $I_{(C1s)}$ was the integrated XPS photoemission intensity of the C 1*s* for a reference fluorocarbon film. Because the ACL was composed of C–C bonding, some of the C–C bonding peaks of the fluorocarbon polymer layer observed for ACL can

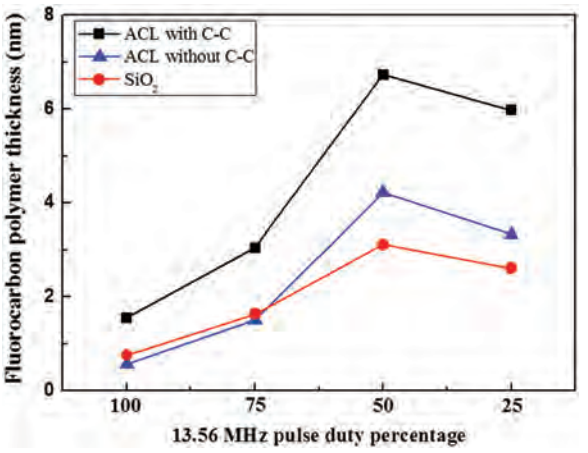

Figure 10. The steady-state thickness of the fluorocarbon polymer on the etched ACL and SiO_2 surface calculated from XPS C 1*s* narrow scan data shown in Figure 9.

be partially related to the C–C bonding from the ACL itself. Therefore, the calculation of the fluorocarbon layer of ACL was carried out with and without the C–C bonding peak intensity in the C 1*s* peak and the results are shown in Figure 10. As shown in Figure 10, the thickness of the fluorocarbon polymer layer on the ACL was generally greater than that on SiO_2 due to the easier removal of CF_x by the formation of CO, CO_2, COF_2, etc., with oxygen in SiO_2 while fluorine is removed by forming SiF_x with silicon in SiO_2. In addition, the fluorocarbon polymer layer thickness was the greatest when the 13.56 MHz pulse duty percentage was 50%. Therefore, the improved ACL critical dimension/thickness and the improved SiO_2 etch profiles observed in Figure 7 at 50% of the pulse duty percentage of 13.56 MHz (that is, at the triple-frequency pulsing with the synchronized pulse on/off) are believed to be related to the thickest fluorocarbon polymer layers formed on the sidewall of SiO_2 and on the top of ACL which is protected from the SiO_2 sidewall etching by the CF_x^+ ion bombardment.

4. CONCLUSION

The effects of 13.56 MHz rf power as a medium frequency for the triple-frequency rf power pulsed CCP composed of 60/13.56/2 MHz on the plasma characteristics and etch characteristics of ACL and SiO_2 were investigated using $Ar/C_4F_6/O_2$ gas mixtures. When the 60/13.56 MHz rf power ratio was varied while keeping the synchronized pulse duty percentage at 50%, the increased ratio of 13.56 MHz rf power increased the electron temperature continuously; however, the dissociation of C_4F_6 showed the highest radical ratios of CF_2/F when the 60/13.56 MHz rf power ratio is 1:1, possibly due to different C_4F_6 dissociation characteristics for different rf frequencies. In addition, the CF_2/F radical ratio was also the highest when the 13.56 MHz pulse duty percentage varied while

maintaining the 60/13.56 MHz rf power ratios of 1:1 and keeping the 60/2 MHz pulse duty percentage at 50%, when 13.56 MHz rf pulse duty percentage is 50%, therefore, at the triple-frequency pulsing conditions with the synchronized pulse on/off. When the CF_2/F ratio was the highest, the highest etch selectivity of SiO_2 over the ACL mask and the most anisotropic SiO_2 etch profiles were observed due to the formation of the thickest fluorocarbon polymer layer formation on the top of the ACL mask and on the sidewall of the etched SiO_2. Consequently, the most anisotropic SiO_2 etch profile was obtained in the triple-frequency CCP system for the rf power conditions of 60/13.56/2 MHz = 200/200/900 W, respectively, and with the synchronized pulse on/off of 50%.

Acknowledgments: This work was supported by the Industrial Strategic Technology Development Program (10041926, development of high density plasma technologies for thin film deposition of nanoscale semiconductor and flexible display processing) funded by the Ministry of Knowledge Economy (MKE, Korea) and also by Samsung Electronics.

References and Notes

1. H. Abe, M. Yoneda, and N. Fujiwara, *Jpn. J. Appl. Phys.* 47, 1435 (**2008**).
2. M. Izawa, N. Negishi, K. Yokogawa, and Y. Momonoi, *Jpn. J. Appl. Phys. Part 1* 46, 7870 (**2007**).
3. T. F. Yen, K. J. Chang, and K.-F. Chiu, *Microelectron. Eng.* 82, 129 (**2005**).
4. T. Goto, K. Ikenaga, A. Teramoto, M. Hirayama, S. Sugawa, and T. Ohmi, *J. Vac. Sci. Technol., A* 26, 8 (**2008**).
5. K. Eriguchi and K. Ono, *J. Phys. D* 41, 024002 (**2008**).
6. A. J. J. Huang, C. C. Min, J. K. Ma, Y. M. Tseng, W. J. Wang, C. M. Wu, C. C. Lin, and T. Y. Huang, *Proc. Dry Process Symp.* (**2006**), p. 263.
7. S. Samukawa, *Appl. Phys. Lett.* 64, 3398 (**1994**).
8. S. Banna, A. Agarwal, K. Tokashiki, H. Cho, S. Rauf, V. Todorow, K. Ramaswamy, K. Collins, P. Stout, J.-Y. Lee, J. Yoon, K. Shin, S.-J. Choi, H.-S. Cho, H.-J. Kim, C. Lee, and D. Lymberopoulos, *IEEE Trans. Plasma Sci.* 37, 1730 (**2009**).
9. K. Tokashiki, H. Cho, S. Banna, J.-Y.Lee, K. Shin, V. Todorow, W.-S. Kim, K. H. Bai, S. Joo, J.-D. Choe, K. Ramaswamy, A. Agarwal, S. Rauf, K. Collins, S. J. Choi, H. Cho, H. J. Kim, C. Lee, D. Lymberopoulos, J. Yoon, W. Han, and J.-T. Moon, *Jpn. J. Appl. Phys.* 48, 08HD01 (**2009**).
10. A. Agarwal, P. J. Stout, S. Banna, S. Rauf, K. Tokashiki, J.-Y. Lee, and K. Collins, *J. Appl. Phys.* 106, 103305 (**2009**).
11. L. Xu, D. J. Economou, V. M. Donnelly, and P. Ruchhoeft, *Appl. Phys. Lett.* 87, 041502 (**2005**).
12. P. Bodart, M. Brihoum, G. Cunge, O. Joubert, and N. Sadeghi, *J. Appl. Phys.* 110, 113302 (**2011**).
13. G. Cunge, D. Vempaire, R. Ramos, M. Touzeau, O. Joubert, P. Bodard, and N. Sadeghi, *Plasma Sources Sci. Technol.* 19, 034017 (**2010**).
14. R. Ramos, G. Cunge, and O. Joubert, *Vacuum* 25, 290 (**2007**).
15. M. D. Logue, H. Shin, W. Zhu, L. Xu, V. M. Donnelly, D. J. Economou, and M. J. Kushner, *Plasma Sources Sci. Technol.* 21, 065009 (**2012**).
16. D. J. Economou, *J. Phys. D: Appl. Phys.* 47, 303001 (**2014**).
17. H. V. Jansen, M. J. de Boer, S. Unnikrishnan, M. C. Louwerse, and M. C. Elwenspoek, *J. Micromech. Microeng.* 19, 033001 (**2009**).
18. M. H. Jeon, A. K. Mishra, S.-K. Kang, I. J. Kim, S. B. Lee, T. H. Shin, and G. Y. Yeom, *Cur. Appl. Phys.* 13, 1830 (**2013**).
19. A. K. Mishra, M. H. Jeon, K. N. Kim, and G. Y. Yeom, *Plasma Sources Sci. Technol.* 21, 055006 (**2012**).
20. N. H. Kim, M. H. Jeon, T. H. Kim, and G. Y. Yeom, *J. Nanosci. Nanotechnol.* 15, 8667 (**2015**).
21. D. Briggs and M. P. Seah (eds.), Practical Surface Analysis by Auger and X-ray Photoelectron Spectroscopy, Wiley, New York (**1983**).
22. B. S. Kwon, J. S. Kim, N.-E. Lee, and J. W. Shon, *J. Electrochem. Soc.* 157, D135 (**2010**).

Received: 27 January 2016. Accepted: 23 March 2016.